

Metal Phosphide Properties and Computational Screens for Ethane Dehydrogenation Catalyst

Jeonghyun Ko[†] and William F. Schneider*,^{†,‡}

†Department of Chemical and Biomolecular Engineering, University of Notre Dame, Notre Dame, IN 46556, United States

‡Department of Chemistry and Biochemistry, University of Notre Dame, Notre Dame, IN 46556, United States

E-mail: wschneider@nd.edu

Table S1: DFT-computed lattice constants.

Element	Hexagonal M ₂ P			Orthorhombic M ₂ P			Pure metal		
	a	b	c	a	b	c	a	b	c
Fe	5.81	5.81	3.42	5.61	3.57	6.51	2.83	2.83	2.83
Co	5.72	5.72	3.40	5.51	3.51	6.58	2.49	2.15	4.03
Ni	5.88	5.88	3.37	5.72	3.54	6.68	3.52	3.52	3.52
Cu	6.16	6.16	3.64	6.10	3.71	7.01	3.64	3.64	3.64
Mo	6.75	6.75	3.25	5.92	4.04	7.32	3.16	3.16	3.16
Ru	6.03	6.03	3.82	5.88	3.88	7.01	2.72	2.35	4.28
Rh	6.10	6.10	3.79	5.88	3.88	7.08	3.82	3.82	3.82
Pd	6.46	6.46	3.64	6.90	3.35	7.71	3.94	3.94	3.94
Ag	6.80	6.80	4.00	6.54	4.08	7.95	4.15	4.15	4.15
Pt	6.80	6.80	3.51	7.00	3.48	7.55	3.97	3.97	3.97

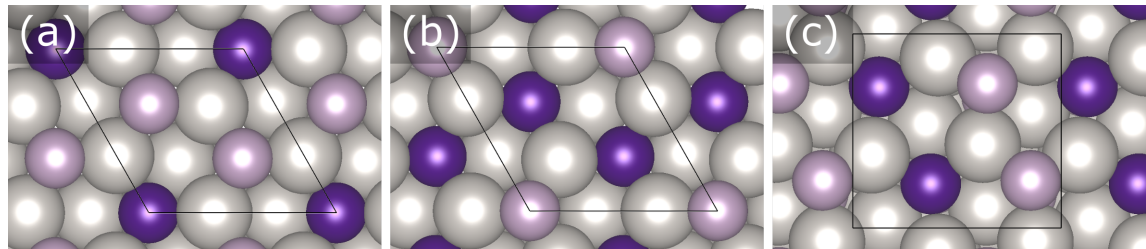


Figure S1: Top views of hexagonal (a) Pt₂P(001)-A, (a) Pt₂P(001)-B, and orthorhombic (c) Pt₂P(010) after geometry optimization. Computational supercells are indicated with light lines, Pt atoms shown in gray, P shown in lavender. Segregated P atoms from sublayer are colored by purple.

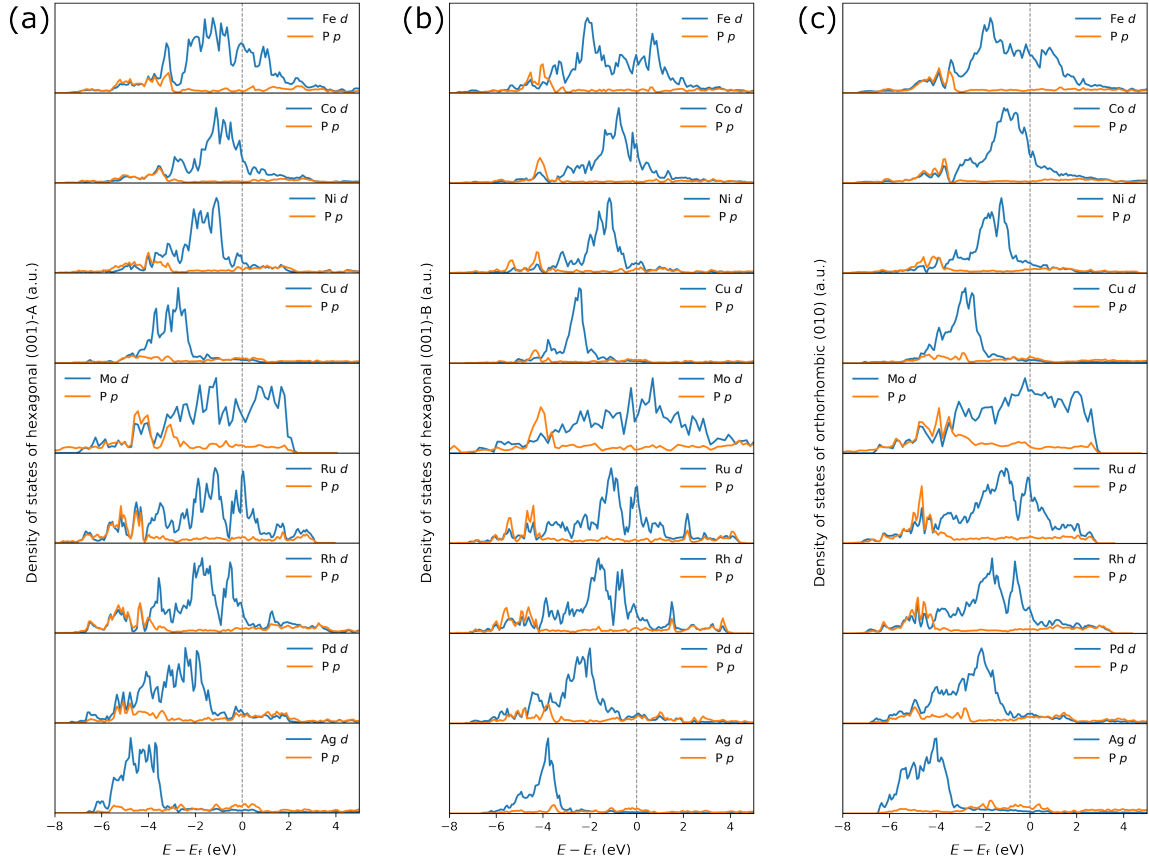


Figure S2: Atom-projected density of states (DOS) of (a, b) hexagonal (001)-A, B and (c) orthorhombic (010) surfaces. The p and d states on the metal and P are shown in blue and orange, respectively.

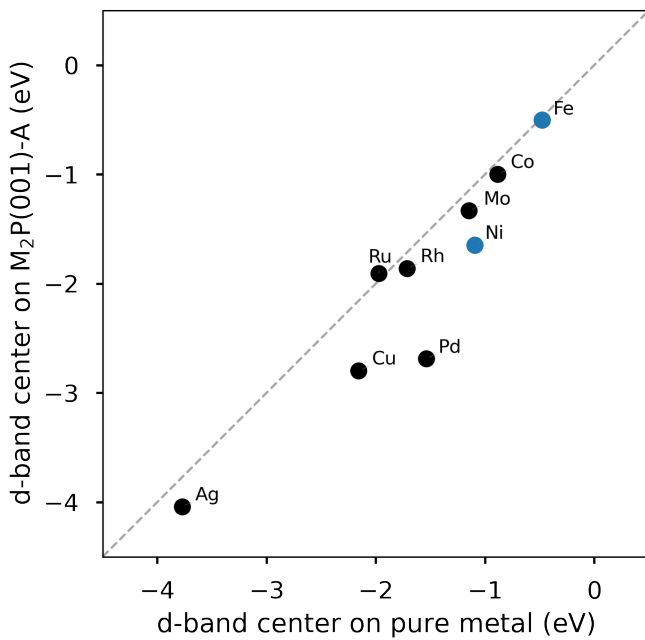


Figure S3: Parity plot of d -band centers (ε_d) of metallic sites on parent metal and $M_2P(001)$ -A. Blue markers highlight compounds that are stable in the hexagonal M_2P structure.

Table S2: *d*-band centers (ε_d) of parent metal and metal atoms on hexagonal M₂P(001)-A, B and orthorhombic (010).

Metal element	Parent metal (eV)	Hexagonal (001)-A (eV)	Hexagonal (001)-B (eV)	Orthorhombic (010) (eV)
Fe	-0.48	-0.50	-0.68	-0.57
Co	-0.88	-1.00	-0.67	-1.04
Ni	-1.09	-1.65	-1.72	-1.72
Cu	-2.16	-2.80	-2.48	-2.74
Mo	-1.15	-1.33	-0.32	-0.86
Ru	-1.97	-1.91	-1.32	-1.69
Rh	-1.71	-1.86	-1.81	-1.86
Pd	-1.54	-2.69	-2.36	-2.51
Ag	-3.77	-4.04	-3.75	-4.04

Table S3: Adsorption energies (E_{ads}) (eV) at M₃-centered site on metal surfaces.

Surface	$E_{\text{ads}}(\text{H})$	$E_{\text{ads}}(\text{C})$	$E_{\text{ads}}(\text{CH})$	$E_{\text{ads}}(\text{CH}_3)$
Fe(110)	-0.70	-8.03	-7.09	-2.17
Co(001)	-0.53	-7.04	-6.45	-1.98
Ni(111)	-0.55	-6.94	-6.56	-1.92
Cu(111)	-0.32	-5.26	-5.38	-1.53
Mo(110)	-0.67	-7.89	-7.36	-2.41
Ru(001)	-0.65	-7.80	-7.10	-2.19
Rh(111)	-0.54	-7.56	-7.00	-1.87
Pd(111)	-0.63	-7.24	-6.65	-1.63
Ag(111)	0.04	-3.98	-4.13	-0.99

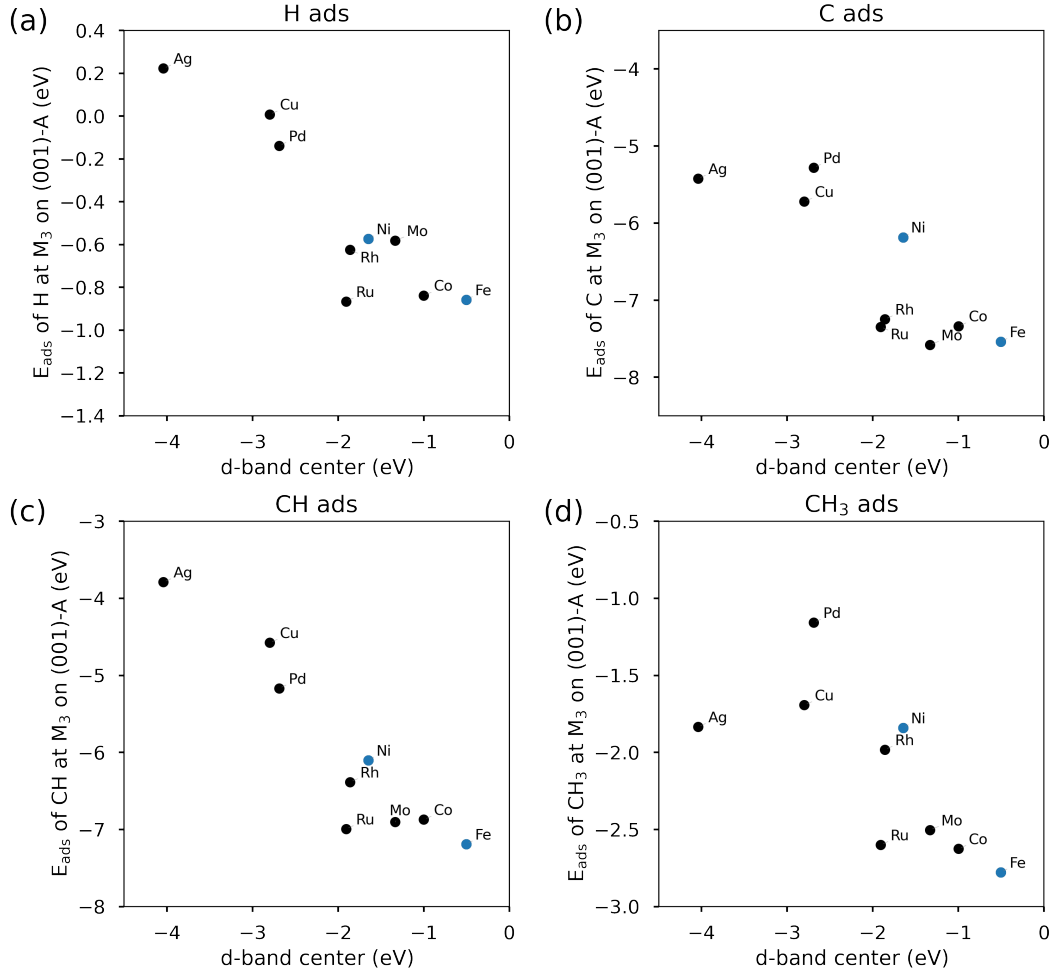


Figure S4: Adsorption energies of (a) H, (b) C, (c) CH and (d) CH₃ plotted against d -band centers (ε_d) of metallic sites on hexagonal M₂P(001)-A. Blue markers highlight compounds that are stable in the hexagonal M₂P structure.

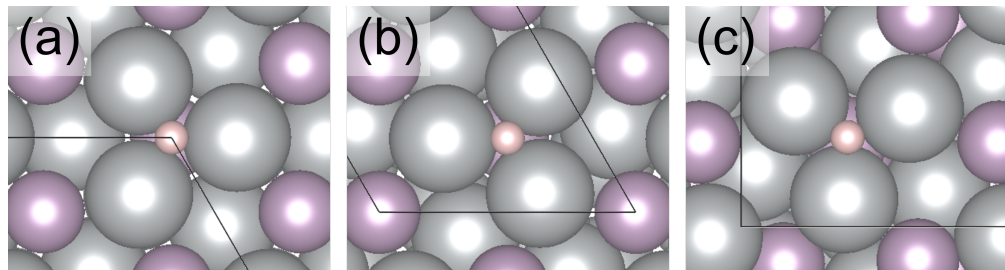


Figure S5: Adsorption geometry of H at M₃-centered sites on hexagonal (a) Ag₂P(001)-A, (b) Ag₂P(001)-B, and orthorhombic (c) Ag₂P(010). Computational supercells are indicated with light lines, H, Ag and P atoms are shown in light pink, gray and lavender.

Table S4: Adsorption energies (E_{ads}) (eV) at M_3 -centered site on hexagonal $\text{M}_2\text{P}(001)\text{-A}$ surfaces.

Surface	$E_{\text{ads}}(\text{H})$	$E_{\text{ads}}(\text{C})$	$E_{\text{ads}}(\text{CH})$	$E_{\text{ads}}(\text{CH}_3)$
$\text{Fe}_2\text{P}(001)\text{-A}$	-0.86	-7.54	-7.19	-2.78
$\text{Co}_2\text{P}(001)\text{-A}$	-0.84	-7.34	-6.87	-2.63
$\text{Ni}_2\text{P}(001)\text{-A}$	-0.57	-6.19	-6.10	-1.84
$\text{Cu}_2\text{P}(001)\text{-A}$	0.01	-5.72	-4.58	-1.69
$\text{Mo}_2\text{P}(001)\text{-A}$	-0.58	-7.58	-6.91	-2.50
$\text{Ru}_2\text{P}(001)\text{-A}$	-0.87	-7.35	-7.00	-2.60
$\text{Rh}_2\text{P}(001)\text{-A}$	-0.63	-7.25	-6.39	-1.98
$\text{Pd}_2\text{P}(001)\text{-A}$	-0.14	-5.28	-5.17	-1.16
$\text{Ag}_2\text{P}(001)\text{-A}$	0.22	-5.43	-3.79	-1.84

Table S5: Adsorption energies (E_{ads}) (eV) at M_3 -centered site on hexagonal $\text{M}_2\text{P}(001)\text{-B}$ surfaces.

Surface	$E_{\text{ads}}(\text{H})$	$E_{\text{ads}}(\text{C})$	$E_{\text{ads}}(\text{CH})$	$E_{\text{ads}}(\text{CH}_3)$
$\text{Fe}_2\text{P}(001)\text{-B}$	-0.53	-7.02	-6.63	-2.18
$\text{Co}_2\text{P}(001)\text{-B}$	-0.70	-7.44	-6.84	-2.21
$\text{Ni}_2\text{P}(001)\text{-B}$	-0.16	-6.21	-5.85	-1.62
$\text{Cu}_2\text{P}(001)\text{-B}$	-0.60	-5.95	-4.95	-1.48
$\text{Mo}_2\text{P}(001)\text{-B}$	-0.93	-7.96	-7.38	-2.91
$\text{Ru}_2\text{P}(001)\text{-B}$	-0.88	-7.86	-7.34	-2.20
$\text{Rh}_2\text{P}(001)\text{-B}$	-0.67	-7.79	-6.61	-1.91
$\text{Pd}_2\text{P}(001)\text{-B}$	-0.06	-5.73	–	-1.19
$\text{Ag}_2\text{P}(001)\text{-B}$	-1.24	–	-4.43	-2.00

Table S6: Adsorption energies (E_{ads}) (eV) at M₃-centered site on orthorhombic M₂P(010) surfaces.

Surface	$E_{\text{ads}}(\text{H})$	$E_{\text{ads}}(\text{C})$	$E_{\text{ads}}(\text{CH})$	$E_{\text{ads}}(\text{CH}_3)$
Fe ₂ P(010)	-0.59	-7.18	-6.74	-2.31
Co ₂ P(010)	-0.65	-7.20	-6.74	-2.27
Ni ₂ P(010)	–	-5.93	-5.60	–
Cu ₂ P(010)	–	-5.79	-4.58	–
Mo ₂ P(010)	-0.94	-8.40	-7.73	-2.90
Ru ₂ P(010)	-0.73	-7.37	-6.98	-2.16
Rh ₂ P(010)	-0.58	-7.16	-6.51	-1.84
Pd ₂ P(010)	–	–	-4.69	–
Ag ₂ P(010)	0.15	–	-4.32	–

Table S7: Adsorption energies (E_{ads}) (eV) at P-centered site on hexagonal and orthorhombic M₂P surfaces.

Surface	$E_{\text{ads}}(\text{CH}_3)$	Surface	$E_{\text{ads}}(\text{CH}_3)$	Surface	$E_{\text{ads}}(\text{CH}_3)$
Fe ₂ P(001)-A	-1.40	Fe ₂ P(001)-B	-1.43	Fe ₂ P(010)	-2.31
Co ₂ P(001)-A	-1.34	Co ₂ P(001)-B	-1.25	Co ₂ P(010)	-1.27
Ni ₂ P(001)-A	-1.90	Ni ₂ P(001)-B	-1.71	Ni ₂ P(010)	-1.67
Cu ₂ P(001)-A	-2.38	Cu ₂ P(001)-B	-1.96	Cu ₂ P(010)	-2.58
Mo ₂ P(001)-A	-1.45	Mo ₂ P(001)-B	-1.70	Mo ₂ P(010)	–
Ru ₂ P(001)-A	-1.74	Ru ₂ P(001)-B	-1.16	Ru ₂ P(010)	-1.72
Rh ₂ P(001)-A	-1.46	Rh ₂ P(001)-B	-1.47	Rh ₂ P(010)	-1.38
Pd ₂ P(001)-A	-2.28	Pd ₂ P(001)-B	-2.18	Pd ₂ P(010)	-3.08
Ag ₂ P(001)-A	-2.75	Ag ₂ P(001)-B	-2.55	Ag ₂ P(010)	-2.53

Table S8: Vibrational frequencies (cm^{-1}) of transition states for ethylene dehydrogenation ($\text{CH}_2\text{CH}_2^* + * \rightarrow \text{C}_2\text{H}_3^* + \text{H}^*$) on hexagonal $\text{Fe}_2\text{P}(001)\text{-A}$.

Normal mode	Vibrational frequency (cm^{-1})	
	path 1	path 2
1	3120	3056
2	3037	3023
3	2025	2087
4	1945	1920
5	1425	1509
6	1359	1211
7	1241	1139
8	993	1024
9	887	865
10	723	816
11	687	756
12	553	577
13	419	438
14	396	364
15	346	331
16	265	269
17	167	231
18	482 i	285 i

Table S9: Vibrational frequencies (cm^{-1}) of transition states for ethylene dehydrogenation ($\text{CH}_2\text{CH}_2^* + * \rightarrow \text{C}_2\text{H}_3^* + \text{H}^*$) on hexagonal $\text{Ni}_2\text{P}(001)$ -A.

Normal mode	Vibrational frequency (cm^{-1})	
	path 1	path 2
1	3039	3122
2	3007	3035
3	2976	2787
4	1905	1931
5	1380	1445
6	1124	1259
7	1052	1147
8	1009	922
9	951	895
10	911	788
11	663	630
12	602	462
13	574	448
14	414	340
15	370	249
16	283	200
17	189	114
18	730 i	678 i

Table S10: Vibrational frequencies (cm^{-1}) of transition states for ethylene dehydrogenation ($\text{CH}_2\text{CH}_2^* + * \rightarrow \text{C}_2\text{H}_3^* + \text{H}^*$) on hexagonal Pd₂P(001)-A.

Normal mode	Vibrational frequency (cm^{-1})		
	Path 1	Path 2	Path 3
1	3129	3128	3112
2	3073	3061	3031
3	3039	3033	2995
4	1568	1570	1418
5	1359	1449	1277
6	1196	1323	1211
7	1171	1155	1174
8	954	1019	960
9	939	927	889
10	879	868	841
11	679	704	635
12	591	481	570
13	422	386	510
14	256	207	347
15	219	150	290
16	80	104	152
17	49	52	110
18	310 i	1005 i	914 i

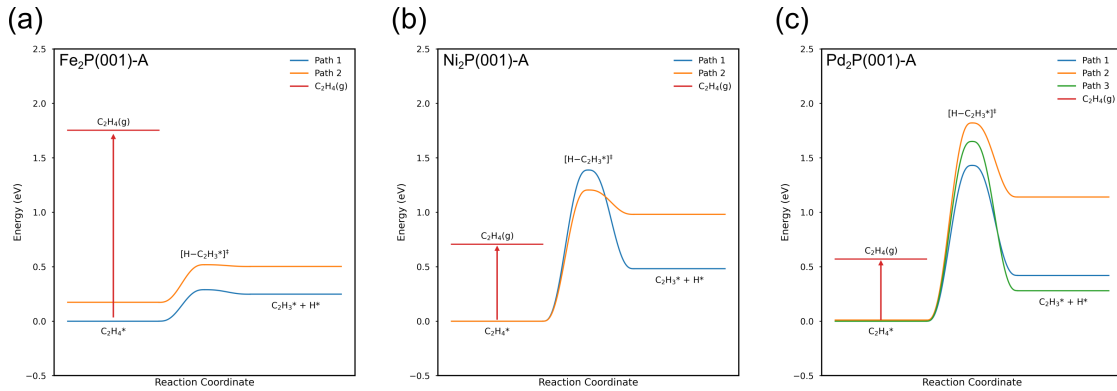


Figure S6: Energy profiles of ethylene dehydrogenation pathways vs ethylene desorption on hexagonal (a) $\text{Fe}_2\text{P}(001)\text{-A}$, (b) $\text{Ni}_2\text{P}(001)\text{-A}$, and (c) $\text{Pd}_2\text{P}(001)\text{-A}$.

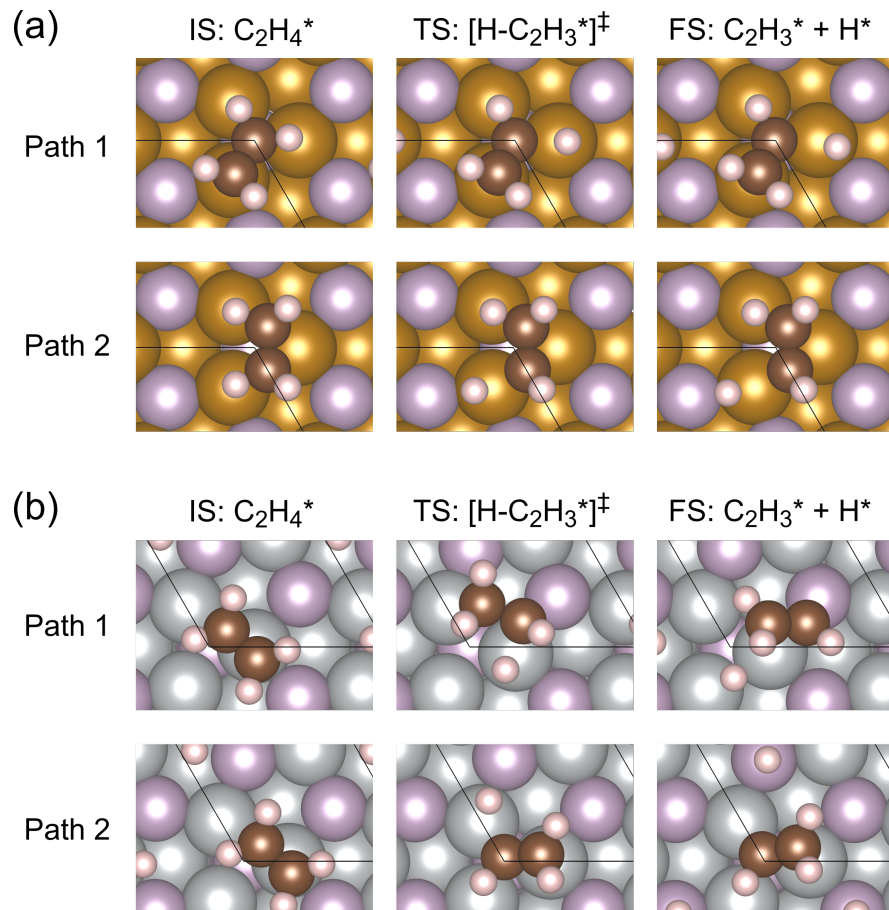


Figure S7: Geometric structures of initial state (IS), transition state (TS) and final state (FS) of possible ethylene dehydrogenation pathways on (a) $\text{Fe}_2\text{P}(001)\text{-A}$ and (b) $\text{Ni}_2\text{P}(001)\text{-A}$.